We are IntechOpen, the world's leading publisher of Open Access books
Built by scientists, for scientists

6,900
Open access books available

186,000
International authors and editors

200M
Downloads

154
Countries delivered to

Our authors are among the

TOP 1%
most cited scientists

12.2%
Contributors from top 500 universities

CLARIVATE ANALYTICS
BOOK CITATION INDEX
INDEXED

WEB OF SCIENCE™

Selection of our books indexed in the Book Citation Index
in Web of Science™ Core Collection (BKCI)

Interested in publishing with us?
Contact book.department@intechopen.com

Numbers displayed above are based on latest data collected.
For more information visit www.intechopen.com

A New Rapid Tooling Process

Xiaoping Jiang and Chao Zhang

1. Introduction

Due to the globalization of the world economy and the consequent increase in competition, it is more important than ever for manufacturers to shorten their product development and manufacturing cycles. The current competitive market not only requires faster product development and reduced production time, but also demands higher quality, greater efficiencies, lower cost, and the ability to meet environmental and recycling objectives.

Tooling is a very important phase in the development and manufacturing of new products and is usually one of the most time-consuming and costly phases. Therefore, shortening the tooling lead-time plays a key role in the re-duction of the overall product development and manufacturing time. Great effort has been made to develop new rapid tooling (RT) technologies that combine the recently emerged rapid prototyping (RP) processes with one or more subsequent processes.

RP normally refers to fabricating prototypes directly from computer aided de-sign (CAD) data using a layered, additive method. Almost all products devel-oped in the manufacturing industry arise from the creation of a three-dimensional computer model using a CAD system. Converting the CAD model into a prototype by using a RP process can be easily realized (Jacobs, 1992). A RP system can quickly generate physical objects and prototypes us-ing liquid, powder, or sheet materials. RP parts allow designers to verify their product design at an early stage and to use three-dimensional representations of the design for sales, marketing and production.

Along with the evolution and improvements of various RP technologies, great research and development efforts have been made in recent years to develop RT technologies based on RP processes (Pham, 1998, Willis, 1997, Hejmadi and McAlea, 1996, Nelson, 1999, and Phelan, 1997). Whether the application is pro-totype, bridge, short-run, or production tooling, RT represents an opportunity to reduce both production time and cost. Therefore, researchers continue to

explore ways to improve RT technologies.

In this study, a new RT process using a metal shell backfilled with metal pow-der to provide mechanical support to the metal shell is presented and the fea-sibility of this new RT process is evaluated. In particular, the study is focused on (1) the packing behavior of the metal powder used to backfill the metal shell, (2) the deformation behavior of the compacted metal powder under compression, (3) the deformation behavior of the metal shell, and (4) the de-formation behavior of the metal shell and compacted metal powder assembly.

2. The New Rapid Tooling Process

The proposed new RT process is shown schematically in Fig. 1. For conven-ience, the figure only illustrates the fabrication of half mould. The proposed new RT process involves the following major steps:

Step 1:   A three-dimensional computer model of the mould is designed on a computer.

Step 2:   A plastic pattern with complementary shape to the mould is fabri-cated using a RP process, such as Stereolithography.

Step 3:   A thin metal layer is deposited onto the cavity side of the plastic pat-tern using an electro-chemical process to form a metal shell. Then, the metal shell is separated from the plastic pattern.

Step 4:   Metal ribs are added to the back of the metal shell to increase the strength of the metal shell.

Step 5:   The metal powder is packed into the metal shell to provide mechani-cal support to the metal shell.

Step 6:   The backside of the mould is sealed to prevent leakage of the metal powder. The tool is finished and ready for moulding operations.

In addition to anticipated short lead-time and low cost, it is also expected that this RT process is environmentally friendly because the metal powder used in backing is fully reusable/recyclable.
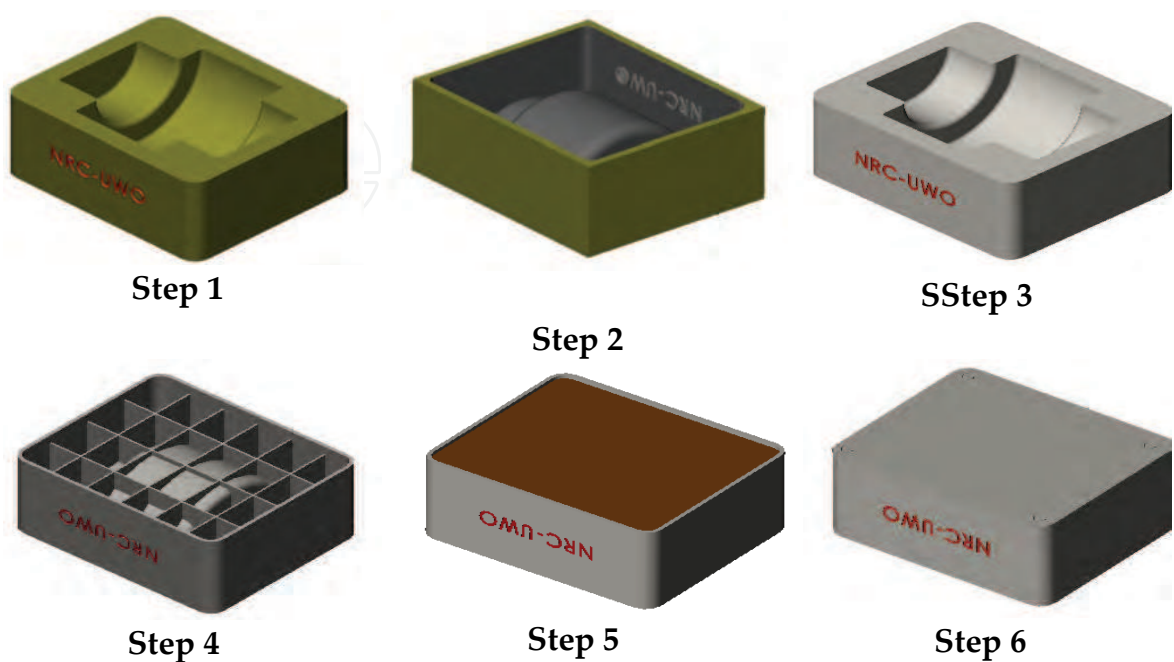
Figure 1. New rapid tooling process

3. Powder Packing Behavior

3.1 Powder Packing Models

Powder packing can be divided into single component packing, binary packing as well as multiple component packing. In single component packing, all packing particles used are of the same size and geometry. In contrast, binary or multiple components packing involves two or more packing components. The powder packing behavior is measured by the packing density, which is defined as the ratio of the volume occupied by the powder to the total volume without compression, i.e.

$$Packing\ Density = \frac{V_{POWDER}}{V_{TOTAL}} = \frac{\sum W_i / \rho_i}{V_{TOTAL}} \qquad (1)$$

where V_{TOTAL} is the total volume of the powder for single component packing or the total volume of the powder mixture for multiple component packing,

W_i is the weight of the powder component i, and ρ_i is the theoretical density of the powder material for component i. In single component packing, packing density of the powder depends on only the packing structure or the arrangement of the particles. In binary and multiple component packing, the packing density is affected by the size and proportion of each packing component. The voids formed by large particles can be filled by small particles. The voids created by small particles can be filled by even smaller particles.

3.2 Procedures for Powder Packing Experiments

For single component powder packing, the powder is first weighed and placed into a scaled cylinder or beaker. The powder in the container is vibrated for 15 minutes on a vibration machine with the topside of the powder being lightly pressed by a flat plate. After vibration, the volume of the powder is measured. The packing density is determined based on the measured data for the weight and volume of the powder.

For binary or multiple component powder packing, the coarse metal powder is weighed and placed into a scaled cylinder. The cylinder is vibrated on a vibrating machine for 15 minutes while the topside of the powder is being lightly pressed by a flat plate. After the volume of the coarse powder is measured, a weighed amount of fine powder is added to the container while the cylinder is vibrated. The volume of the mixed powders is measured and the packing density of the mixed powders is calculated. For a three-component mixture, the weighted finer powder is added to the previous mixture while the cylinder is vibrated. The final volume is measured and the packing density of the mixed powders is calculated.

For binary component powder packing involving low fluidity powders, the weighed coarse and fine powders are placed into a scaled cylinder or a beaker. The mixture is stirred so that the powders are mixed evenly. It is then vibrated. The volume of the mixed powders is measured after the vibration. The packing density is calculated.

In this study, eleven different metal powders are selected for the powder packing experiment. The particles of the selected powders have different shapes and sizes, and they are made of different materials. The characteristics of the selected powders are listed in Table 1.

Powder number	Powder name	Material	Material density (g/ml)	Geometry	Average particle size (μm)
1	Carbon Steel Ball	Carbon Steel	7.85	Spherical	3175
2	12 HP Copper Shot	Copper	8.91	Round	850
3	34 HP Bronze	Bronze	8.65	Round	450
4	Fe	Iron	7.85	Spherical	22~53
5	T-15	Tool Steel	8.19	Spherical	>150
6	T-15	Tool Steel	8.19	Spherical	80~150
7	T-15	Tool Steel	8.19	Spherical	<22
8	ATOMET 1001	Low Carbon Steel	7.85	Irregular	>150
9	ATOMET 1001	Low Carbon Steel	7.85	Irregular	<22
10	DISTALOY 4600A	Low Carbon Steel	7.9	Irregular	>150
11	DISTALOY 4600A	Low Carbon Steel	7.9	Irregular	<22

Table 1. Characteristics of selected powders

3.3 Results of the Single Component Powder Packing Experiments

The packing density depends on the characteristics of the particles. Generally, for powder packing, the density of the powder material has no significant influence on its packing density. Particles of the same size and shape will have the same packing density despite of the difference in their theoretical densities (Leva and Grummer, 1947). The main factors affecting the packing density for single component powder packing are particle size, particle shape, and the ratio of the diameters of the container to the particle.

(a) The effect of the ratio of the diameters of the container to the particle

McGeary (1962) studied the effect of the ratio of the diameters of the container to the particle D/d (D is the container diameter and d is the particle diameter) and concluded that if the ratio D/d is greater than 50, the packing density tends to reach the maximum value. Experiments are carried out here for ratios D/d

from 3.5 to 39.4 using 3175 μm (1/8-inch) diameter carbon steel balls (Powder #1) and for the ratio D/d of 57.6 using 12 HP copper shorts of diameter of 850 μm (Powder #2). In the carbon steel ball packing tests, different diameter containers are used to create different D/d ratios. The experimental results presented in Table 2 show the effect of the ratio D/d on the packing density. The lowest packing density, 0.55, occurs at the lowest ratio D/d, which is 3.5. The highest packing density is 0.65 when the ratio D/d is 57.6. It can be observed from Table 2 that the packing density increases with the increase of the ratio D/d. However, the packing density does not change much when the ratio D/d is greater than 7.66.

Powder number	2	1	1	1	1	1	1
D/d	57.6	39.4	15.1	10.9	7.66	4.93	3.50
Packing density	0.65	0.63	0.61	0.62	0.62	0.58	0.55

Table 2. Single component packing density for different D/d

(b) The effect of the particle shape

The particle shape varies significantly depending on the manufacturing process used and influences the particle packing, flow, and compression properties. The greater the particle surface roughness or the more irregular the particle shapes, the lower the packing density (Shinohara, 1984). For a gas atomized metal powder, the shape is almost spherical and for water atomized metal powder, the shape is more irregular (German, 1998). Some particle shapes of the selected powders used in this study are shown in Fig. 2.

Table 3 gives the comparison of the packing densities for powders with different particle shapes. The powders with irregular particle shapes, DISTALOY 4600A (Powders #10 and #11) and ATOMET 1001 (Powders #8 and #9) powders, have a lower packing density, which is 0.49, as compared with the packing density of the powders of the spherical shape with the same size (Powders #5 and #7), which is 0.63. Therefore, the packing density of the powders with irregular shapes is 22% lower than that of the powders with the spherical shape.

(c) The effect of the particle size

The results shown in Table 3 also indicate the effect of the particle size on the packing density of the powder. It can be seen that the packing densities for the

powders with spherical shape and round shape are between 0.60 and 0.63, and it is 0.49 for the powders with irregular shapes, despite of the difference in the particle size. Thus, particle size has no significant effect on the packing density. However, a test for the particle fluidity by pouring the powders onto a plate with smooth surface that is at a 45° angle to the horizontal plane reveals that the particles demonstrate a low fluidity if the particle size is less than 22 μm.

Powder number	1	2	3	4	5	6
Shape	Spherical	Round	Round	Spherical	Spherical	Spherical
Size (μm)	3175	850	450	22~53	>150	80~150
Packing density	0.63	0.65	0.63	0.63	0.63	0.60
Powder number	7	8	9	10	11	
Shape	Spherical	Irregular	Irregular	Irregular	Irregular	
Size	<22	>150	<22	>150	<22	
Packing density	0.63	0.49	0.49	0.49	0.49	

Table 3. Single component packing density for different particle shapes and sizes

ATOMET 1001   DISTALOY 4600 A   T-15

├──┤
100 μm
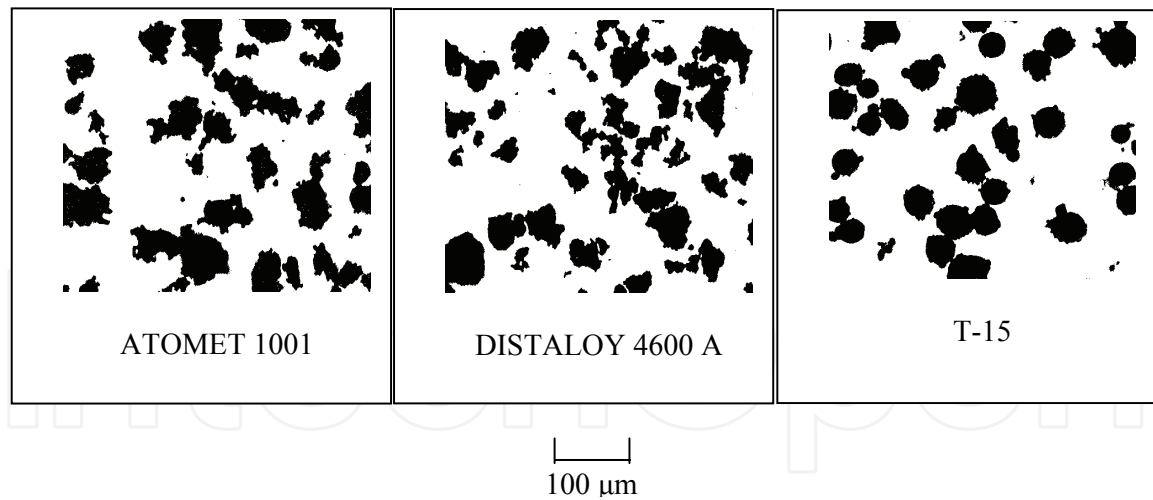
Figure 2. Optical micrographs of powders with different shapes

3.4 Results of the Binary and Tertiary Powder Packing Experiments

The results of the single component powder packing experiments indicate that the maximum packing density is about 0.65. For the new RT process considered in the current study, a higher packing density is required to achieve sufficient load transfer ability. Adding certain amount of smaller particles into a

packing structure consisted of large particles can greatly improve the packing density. Small particles are used to fit into the interstices between large particles, and smaller particles can be used to fit into the next level of pores. Thus, the packing density can be improved. This is the basic principle for the binary or multiple component packing. The factors that affect the binary or tertiary packing density, such as the size ratio and the mixing ratio of the packing components, are considered in this study. The mixing ratio is defined as the ratio of the weight of the large particle to the total weight of the powder mixture and the particle size ratio is defined as the ratio of the size of the large particle to the size of the small particle.

(a) The effect of the particle size ratio

To exam the effect of the particle size ratio of the packing components on the packing behavior of binary and tertiary mixtures, the experiments are conducted for different particle size ratios at the mixing ratio of 0.74 for binary mixtures, and 0.63 for the large size particles in the tertiary mixture and 0.23 for the middle size particles in the tertiary mixture. Table 4 gives the packing densities of binary and tertiary mixtures at different particle size ratios. The results show that adding small particles into a packing structure of large particles can greatly increase the packing density. The packing density of the binary or tertiary mixture increases between 9% and 44% as compared with the single component packing density. The increase in the packing density for the binary mixture with a low particle size ratio (Cases 4-6) is in the range of 9% ~ 14% and it is 32% ~ 33% for the binary mixture with a high particle size ratio (Cases 2 and 3).

Case	Powder mixture	Particle size ratio	Packing density			Packing density increase (%)
			Large particle	Small particle	Mixture	
1	#1+#3+#7	144: 20.5: 1	0.63	0.63	0.91	44
2	#1+#4	(59.9~144): 1	0.63	0.63	0.84	33
3	#2+#4	(16.0~38.6): 1	0.65	0.63	0.86	32
4	#5+#7	6.82: 1	0.63	0.63	0.71	13
5	#2+#6	(5.67~10.6): 1	0.65	0.60	0.71	9
6	#1+#2	3.74:1	0.63	0.63	0.72	14

Table 4. Binary and tertiary packing density for different particle size ratios

The increase in the packing density for the tertiary mixture is 44%. The basic requirement of good multiple component packing is that small particles can freely pass through the voids between large particles. For spherical component packing, the minimum size ratio that satisfies this requirement can be determine using the packing models shown in Fig. 3.

There are two extreme packing conditions in the ordered single component packing. The simple cubic packing, as shown in Fig. 3 (a), produces the largest interstice between particles. The face-centered cubic packing shown in Fig. 3 (b), on the other hand, produces the smallest interstice between particles. The size of the fine particles should be smaller than the throat gate dimension of large particles so that the fine particles can freely pass through the throat gate between large particles. In Fig. 3, R is the radius of the large sphere, and r is the radius of the small sphere. For the face-centered packing model, the relation between R and r can be expressed as:

$$\frac{R}{R+r} = \cos 30° \qquad\qquad (2)$$

(a)   (b)
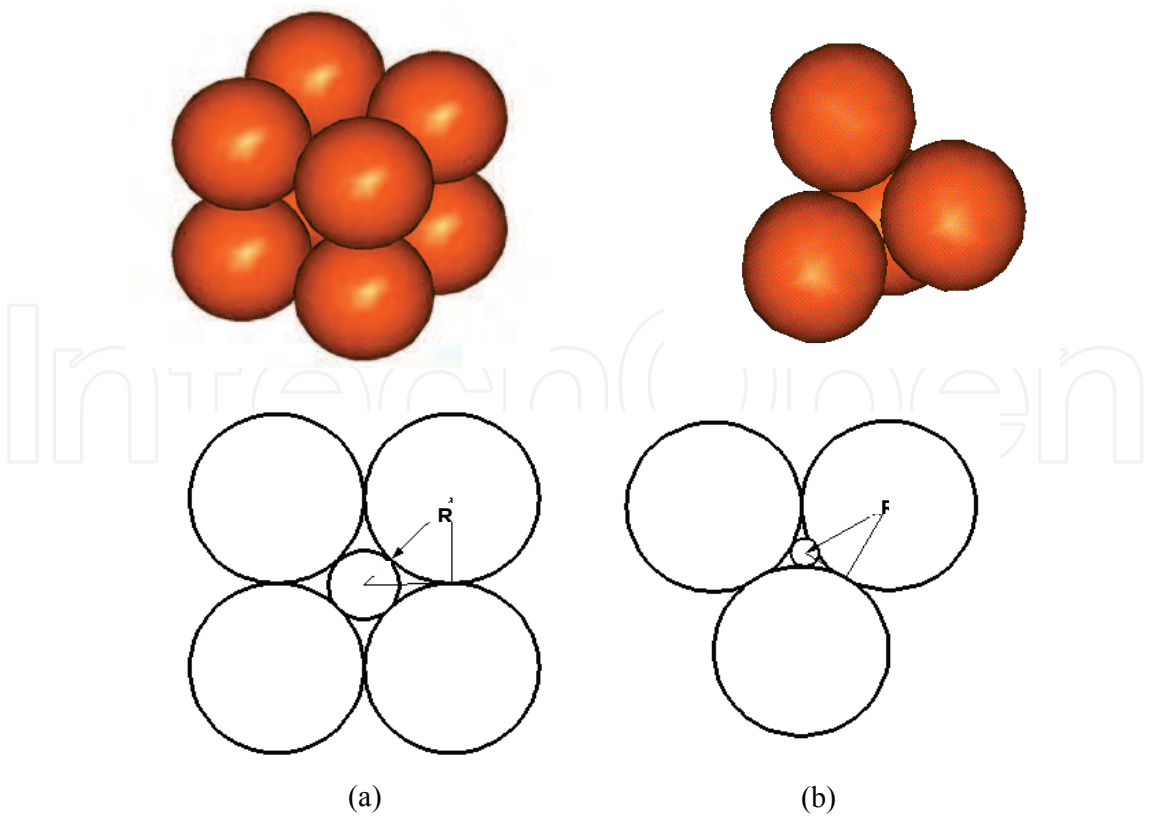
Figure 3. Throat gate structures between particles. (a) Simple cubic packing; (b) Face-centered cubic packing

From Eq. (2), we have $R/r = 6.46$. For the simple cubic packing, the relation becomes

$$\frac{R}{R+r} = \cos 45° \qquad (3)$$

Therefore, $R/r = 2.41$

It can be concluded that the minimum particle size ratio, R/r, for small particles to fill the voids between large particles without pushing them apart is 2.41. When the ratio R/r is greater than 6.46, all of the small particles can pass the throat gates and enter the interstices between large particles. In order to obtain a higher packing density, the particle size ratio should be greater than 6.46.

The experimental results shown in Table 4 reflect the effect of particle size ratio. The particle size ratios in Cases 1 to 3 are much higher than 6.46. Thus, the packing densities in these cases are higher than those in Cases 4 to 6. In Case 6, the particle size ratio is lower than 6.46, but higher than 2.41. So, the small particles can only partially fill the voids between the large particles. The packing density increases compared with the single component packing density. However, it is lower than that with high particle size ratio. In Case 5, the size ratio varies from 5.67 to 10.6 and it does not totally satisfy the particle size ratio requirement for good binary packing, which leads to a lower packing density. The particle size ratio in Case 4 is 6.82 and it is greater than the minimum particle size ratio requirement for good binary packing, which is 6.46 based on ordered packing. However, the packing density is also low. This is due to the fact that the actual powder packing is not ordered packing. The result suggests that the minimum particle size ratio for actual powder packing to achieve a good binary packing should be higher than 6.82. As expected, the highest packing density is obtained from tertiary powder packing, Case 1, which is 0.91.

It is observed that the binary packing density for the mixture of Powder #2 and Powder #4 (Case 3) is slightly higher than that for the mixture of Powder #1 and Powder #4 (Case 2). This may attribute to the fact that the single component packing density for Powder #1 is lower than that for Powder #2 as shown in Table 3. It is also noticed that the binary packing density is between 0.71 and 0.72 when the particle size ratio is lower than the minimum particle size ratio requirement for good binary packing and it is 0.84 to 0.86 when the particle size ratio is higher than the minimum particle size ratio requirement. Therefore, the particle size ratio has little effect on the binary packing density

once the size ratio is lower or higher than the minimum particle size ratio requirement for good binary packing.

(b) The effect of the mixing ratio

The experiments are conducted for binary mixtures at different mixing ratios to investigate the effect of the mixing ratio on the packing density of binary powder mixtures. Table 5 shows the experimental results of packing densities for four different binary mixtures at different mixing ratios. The packing density varies from 0.67 to 0.86. It can be seen from the results that there is an optimal mixing ratio for each binary mixture at which the packing density of the binary mixture is maximal.

When small particles are added to fill the voids between the large particles, the porosity of the binary powder mixture decreases. Therefore, the packing density of the binary mixture increases. When the small particles fill all of the voids without forcing the large particles apart, the packing density of the binary mixture is at its maximum value. Further addition of small particles will force the large particles apart and the packing density will decrease. The optimal mixing ratio falls in the range of 0.71 - 0.77.

Mixture	#2+#6	#1+#4	#2+#4	#5+#7
Particle size ratio	5.67~10.6	59.9~144	16.0~38.6	6.82
Mixing ratio	Binary packing density			
0.65	0.70	0.82	0.83	0.68
0.68	0.71	0.82	0.84	0.69
0.71	0.72	0.83	0.85	0.70
0.74	0.71	0.84	0.86	0.71
0.77	0.70	0.82	0.86	0.72
0.80	0.69	0.81	0.85	0.70
0.83	0.68	0.80	0.83	0.68
0.86	0.67	0.77	0.80	0.67

Tabele 5. Binary packing density at different mixing ratios

4. Deformation Behaviour of Compacted Metal Powder under Compression

The effects of various parameters on the deformation behavior of compacted metal powder under compressive loading are investigated experimentally in

order to examine the feasibility of the proposed new RT process. The experimental results are used to obtain the elastic properties of the compacted metal powder under various loading conditions. These are important parameters for the deformation analysis of the metal shell and powder assembly used in the new RT process.

4.1 Compression Experiments

The metal powders used for the compression experiments are given in Table 6. Three different kinds of powders are selected to provide different particle shapes and hardness. As shown in Table 6, T-15 tool steel powder has much higher hardness than that for ATOMET 1001 and DISTALOY 4600A. For T-15, both coarse and fine size particles are used to examine the compression behaviour of powder mixtures. For ATOMET 1001 and DISTALOY 4600A, only coarse size particles are used. The sizes of the powders are chosen so that the size ratio of coarse powder and the fine powder is greater than 7. The mixing ratio of the coarse and fine powders is varied between 0.70 and 0.80, which gives a higher packing density as shown in Table 5. The compression tests are carried out using an Instron Mechanical Testing System according to ASTM standard B331-95 (ASTM B331-95, 2002) in an axial compression die shown schematically in Fig. 4. The powder is dried in an oven at 105oC for 30 minutes before the compression test to remove any absorbed moisture. The powder is vibrated for 15 minutes in the single component powder compression test after being loaded into the compression die.

Powder	Particle size		Material properties				Shape
	Coarse (μm)	Fine (μm)	ϱ (g/ml)	E (GPa)	HRB	ν	
T-15	150-350	6- 22	8.19	190~210	220	0.27~0.3	Spherical
ATOMET 1001	45-150	-	7.85	190~210	48	0.27~0.3	Irregular
DISTALOY 4600A	45-150	-	7.85	190~210	79	0.27~0.3	Irregular

Table 6. Characteristics of selected powders ϱ – Density; E - Young's modulus; HRB – Hardness; ν -Poisson's ratio

The coarse and fine powders are carefully mixed in the die and are then vibrated for 15 minutes before the compression test of the mixed powders. The loading and unloading rate is 10 kN/min, and the maximum compressive stress used is 138 MPa, corresponding to the maximum injection moulding pressure used for forming most engineering plastics.

4.2 Results

(a) The effect of powder material properties on powder compressive properties

Table 7 shows the results of the single loading-unloading compression experiments for the three coarse powders listed in Table 6. The powder compact density is defined as the ratio of the volume occupied by the powder to the total volume after the compression. It can be seen that the powder material properties have a significant effect on the compressive characteristics of the powder. The total strain under the same loading condition for the T-15 tool steel powder is 0.157, which is the smallest among all powders considered.

Powder (coarse)	Total strain	Compact density	Packing density	Powder condition after compression
T-15 Tool Steel	0.157	0.627	0.63	Loose
DISTALOY 4600A	0.375	0.692	0.49	Block
ATOMET 1001	0.462	0.766	0.49	Block

Table 7. Effect of powder material properties on powder compressive deformation behavior

In contrast, the total strain for the ATOMET 1001 powder is largest, 0.462, three times that of the T-15 tool steel powder. For the purposes of comparison, the packing density obtained in Section 3 is also listed in Table 7. It can be seen that the change between the powder compact density and packing density is smallest for the T-15 tool steel powder that corresponds to the smallest total strain. Therefore, as expected, powders with higher hardness produce smaller compressive strain and density change under the same compressive load.
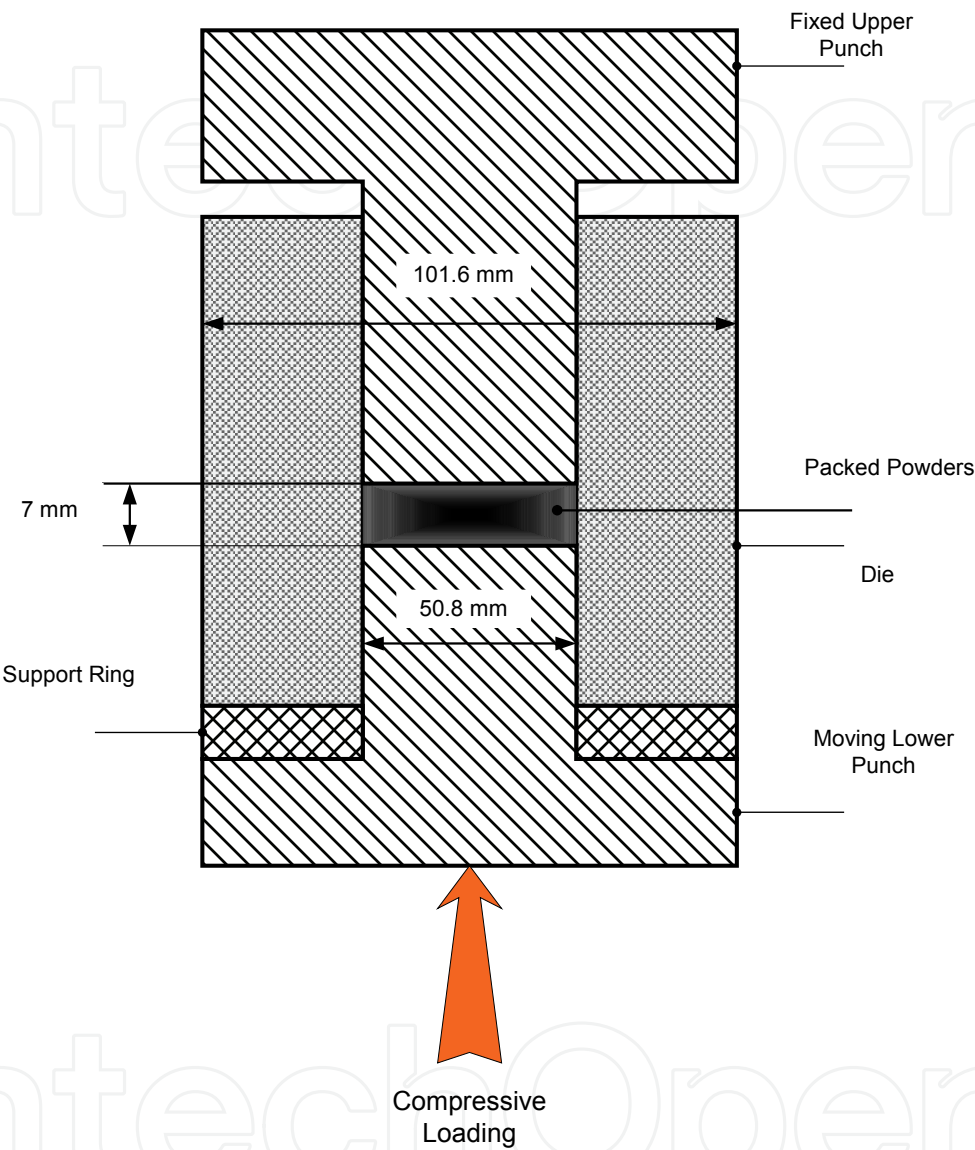
Figure 4. Die and punches for the compression test

It is also observed that the T-15 tool steel powder has the lowest compact density after compression although it has the highest packing density before compression. Therefore, for the same powder compact density, harder materials can support bigger loads. This suggests that powders with high hardness are preferred for the backing application in the proposed new RT process. In addition, the test indicates that soft powders such as DISTALOY 4600A and ATOMET 1001 tend to form blocks after compression. Such powder blocks cannot be reused for tooling applications because they lose the filling capabil-

ity that powders possess. In contrast, the T-15 tool steel powder remains in loose condition after compression at a compression stress of up to 138 MPa. Such powders are better choices for the application in the proposed new RT process from a reusable point of view. Therefore, the T-15 tool steel powder is used in the experiments conducted in subsequent sections.

(b) The effect of the mixing ratio on the compressive properties of binary powder mixtures

The RT process considered in the current study requires a higher packing density to achieve sufficient load transfer ability. The addition of smaller particles into a packing structure consisting of large particles can greatly improve the packing density. Experiments that involve the binary powder mixture of the coarse T-15 powder and fine T-15 powder at different mixing ratios using a single loading-unloading compression cycle are also carried out. The mixing ratio is defined as the ratio of the weight of the coarse powder to the total weight of the powder mixture. Table 8 shows the total compressive strain and corresponding powder compact density of the binary powder mixture at different mixing ratios. It can be seen from the results that at the mixing ratio of 0.77, the total strain is minimal and the compact density is maximum. This is also the optimal mixing ratio for T-15 tool steel powder mixture at which the powder packing density is maximal as shown in Table 5. It is clear that the optimal mixing ratio corresponding to a maximum powder packing density produces the least compressive deformation.

(c) Compressive behavior of powders in multiple loading-unloading cycles

To investigate the effect of loading history on the deformation behavior of the compacted metal powder, multiple loading-unloading experiments for the T-15 binary powder mixture with a mixing ratio of 0.77 are carried out using a five-cycle loading pattern shown in Fig. 5.

Powder Mixture	Mixing Ratio	Total Strain	Compact Density
T-15 Tool Steel	0.80	0.183	0.783
T-15 Tool Steel	0.77	0.162	0.822
T-15 Tool Steel	0.74	0.179	0.810

Table 8. Effect of the mixing ratio on binary powder compressive deformation behavior
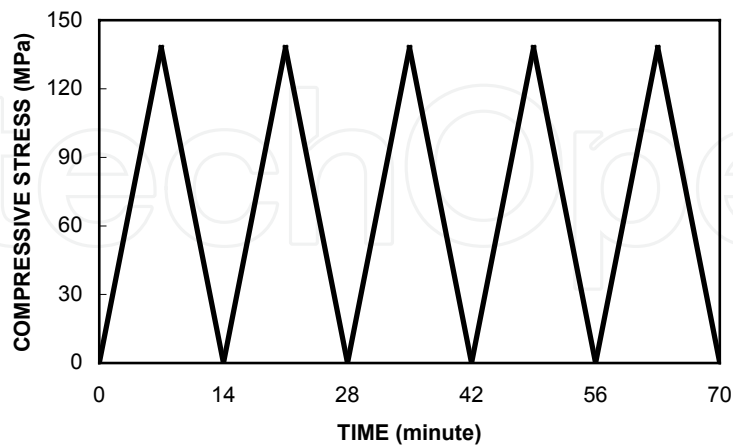
Figure 5. Loading pattern of the five-cycle compression test

(i) Loading history and critical point

The loading-unloading curves for the five-cycle compression test are shown in Fig. 6. The first loading curve is significantly different from the succeeding unloading and reloading curves. For the same load, it showed that the total deformation is twice as much as the other curves. Upon unloading during the first cycle, approximately 50% of the deformation is recovered, indicating a large amount of irreversible deformation during the first load cycle. After the unloading, the next reloading curve crosses the previous unloading curve at a certain stress level.
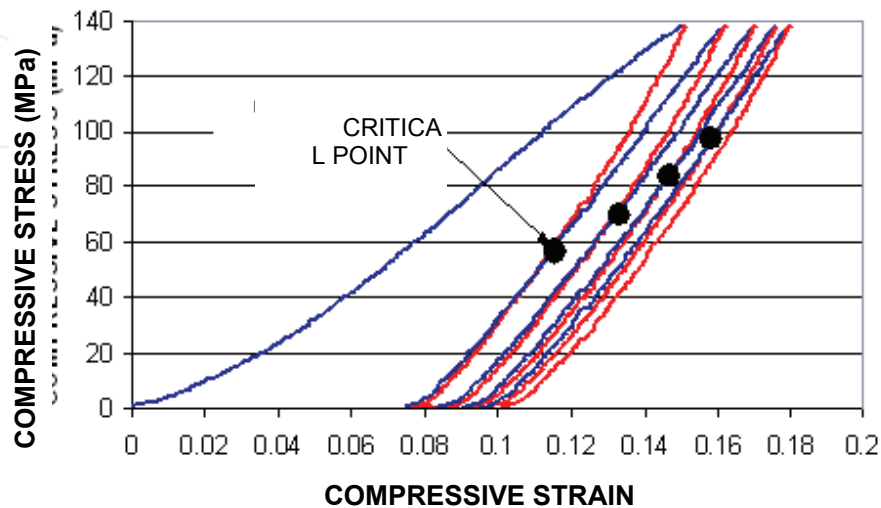
Figure 6. Typical loading-unloading curves of the five-cycle compression test

A pair of unloading and subsequent reloading curves form a cross point, as shown in Fig. 6. This cross point is referred to as the critical point. The unloading and reloading curves become parallel and closer to each other as the reloading and unloading cycles proceed. The tangent of the unloading or the reloading curve increases over cycles and approaches a constant value.

The critical point has two features. First, when the load is below the critical point, the reloading curve lies on the left side of the unloading curve of the previous cycle and the two curves essentially overlap with each other, indicating that the deformation below the critical point is mostly elastic in nature. On the other hand, when the reloading load goes beyond the critical point, the strain of reloading exceeds that in the previous unloading process, and the curves shows a hysteresis. Secondly, the stress corresponding to the critical point moves higher with an increased number of cycles, as shown in Fig. 6.

The deformation behavior and the critical point phenomenon can be understood from the deformation mechanisms of the powder compact. During the first loading cycle, the vibration packed powder particles only have point contacts with each other and will go through a large amount of irreversible deformation through such mechanisms as relative particle movement, plastic deformation at contacting points, and perhaps particle fracture for brittle particles (Carnavas, 1998). Elastic deformation will increase with the increase in the load and the decrease in the irreversible deformation. Upon unloading in the first load cycle, only the elastic component of the deformation is recovered, leaving a significant amount of irreversible deformation. During the succeeding loading cycles, the irreversible deformation mechanisms have largely been exhausted, and therefore a major portion of the deformation is elastic in nature. In particular, when the load is below the critical point, the deformation is essentially elastic and completely reversible. However, when load is high enough, i.e., beyond the critical points, some of the irreversible deformation mechanisms, such as local plastic deformation and particle relative movements, can further contribute to the unrecoverable deformation. It can be expected that with the proceeding of repeated loading-unloading cycles, the available sites and the amount of irreversible deformation will be gradually reduced, and therefore resulting in increased critical point and tangent of the loading-unloading curves.

These features indicate that the elastic properties of compacted powders can be controlled with properly designed loading-unloading cycles.

(ii) The effect of the mixing ratio on the critical point

Figure 7 shows the effect of the binary mixing ratio on the position of the critical point. The compressive stresses corresponding to the first and the fourth critical points are shown in Table 9. It can be seen that the binary powder mixture with a mixing ratio of 0.77 has higher critical points compared to the powder mixtures with mixing ratios of 0.74 and 0.80, respectively. The mixing ratio of 0.77 corresponds to the highest powder packing density in the binary packing system. A higher critical point means a higher deformation resistance in the subsequent reloading. High deformation resistance is beneficial for maintaining the integrity of tooling under working conditions for the intended RT application.

(d) The effect of loading history on the compressive properties of binary powder mixtures

Excessive deformation of compacted powders in the proposed RT application is undesirable and must be avoided. To minimize the deformation of the power compacts under repeated compressive load cycles, two new compression tests are designed and carried out to examine the deformation behavior of compacted powders under cyclic loading below the critical point using the binary T-15 tool steel powder mixture. The loading patterns for the two tests are shown in Figs. 8 and 9, respectively.

In the first test, after two cycles of loading and unloading at the maximum load of 138 MPa, three more cycles of loading-unloading are added with a maximum load set at 60% of the previous maximum load, as shown in Fig. 8.
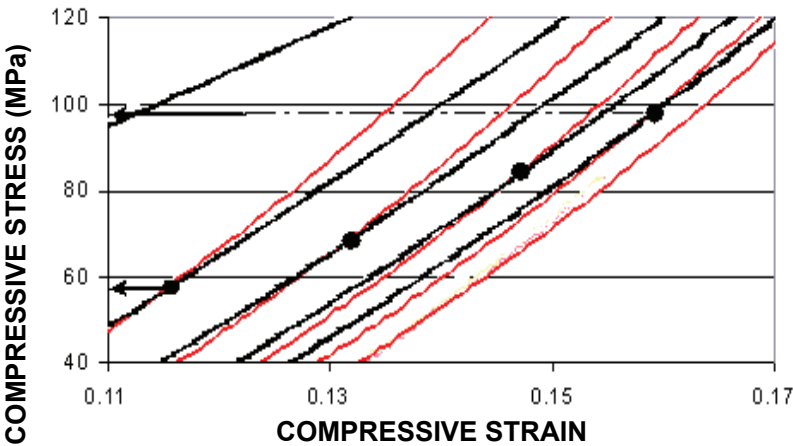
(a) Mixing ratio: 0.74
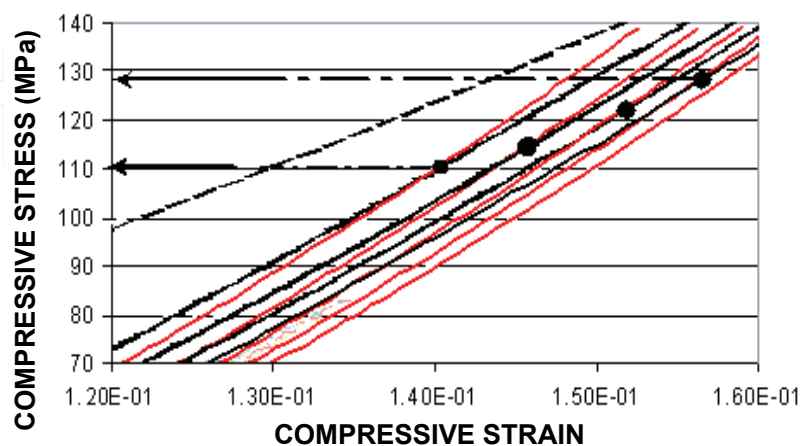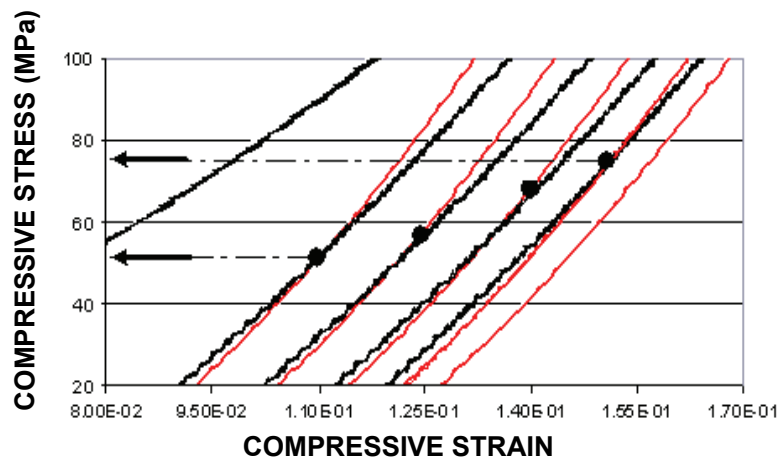
(b) Mixing ratio: 0.77

(c) Mixing ratio: 0.80

Figure 7. Locations of critical points

The new maximum load after initial loading was chosen as 60% of the initial maximum load so that the it is safely below the critical points on the initial loading curves (The stresses at critical points are at least 80% of the maximum load for the mixture with a mixing ratio of 0.77 as shown in Fig. 7b) and still practical for injection moulding of engineering plastics.

In the second test, the powder first undergoes five loading and unloading cycles with a maximum load of 138 MPa, and three more cycles are followed with the maximum load set at 60% of that used in previous cycles, as shown in Fig. 9. Figure 10 shows the loading-unloading curves of the compression test using the loading pattern shown in Fig. 8 and powder mixtures with mixing

ratios of 0.74, 0.77, and 0.80, respectively. For all mixing ratios studied, there is no further strain increase observed in the three loading-unloading cycles with reduced maximum load. Details of the stress-strain curves for the mixing ratio of 0.77 are given in Fig. 11. Figure 12 shows the experimental results using the second loading pattern shown in Fig. 9. Again, there is no further increase in the total strain observed in the three loading-unloading cycles with reduced maximum load.

Powder mixture	Mixing ratio	At the first critical point (MPa)	At the fourth critical point (MPa)
T-15 tool steel	0.80	52	75
T-15 tool steel	0.77	110	127
T-15 tool steel	0.74	58	98

Table 9. Compressive stress at the first and fourth critical points
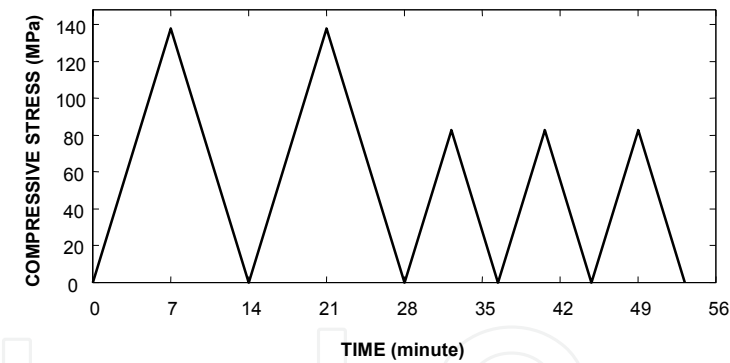
Figure 8. First loading pattern
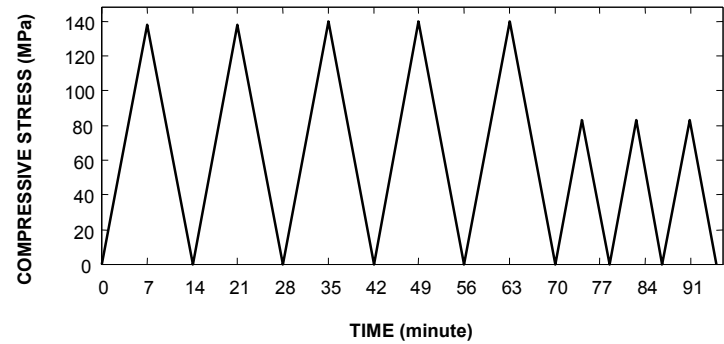
Figure 9. Second loading pattern
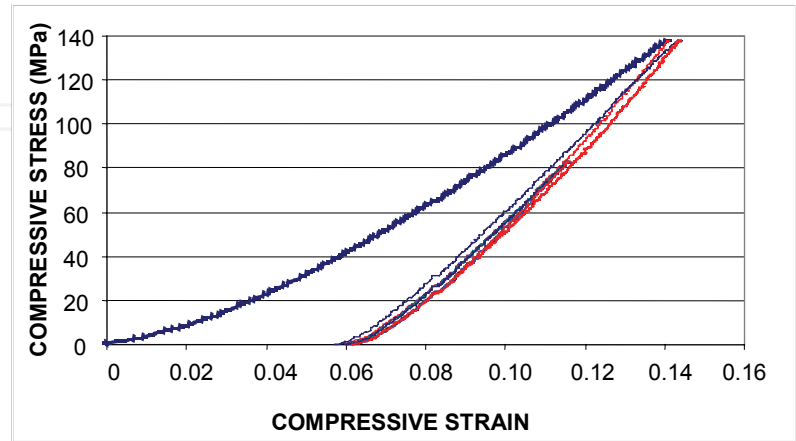
(a) Mixing ratio 0.74
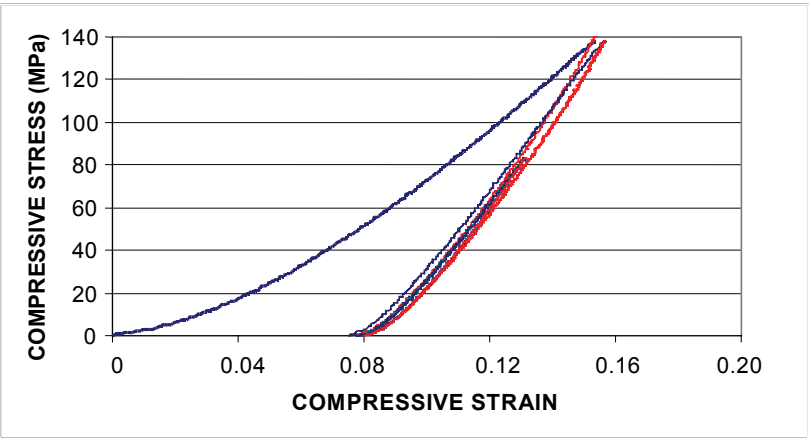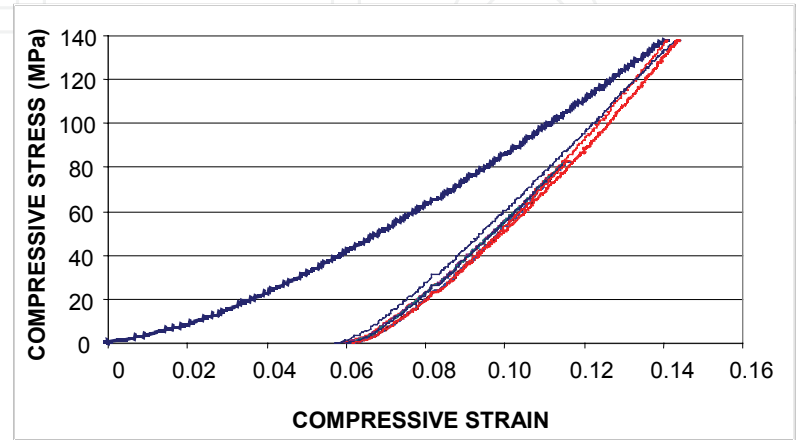
(b) Mixing ratio 0.77

(c) Mixing ratio 0.80

Figure 10. Loading-unloading curves using the first loading pattern

These results indicate that by properly pre-compressing the metal powders, plastic deformation of the backing metal powders can be eliminated in the proposed RT process. It is also seen that the increase in the total strain in the first five loading-unloading cycles is smallest for the mixing ratio of 0.77 among all powder mixtures examined. This is consistent with the results from the compression test using a single loading-unloading cycle.

Table 10 shows the change in total strain and powder compact density between the second loading and the last loading for the loading pattern shown in Fig. 9. It is seen that the powder mixture with a mixing ratio of 0.77 has the least increase in both the total strain and powder compact density between the second loading and the last loading.
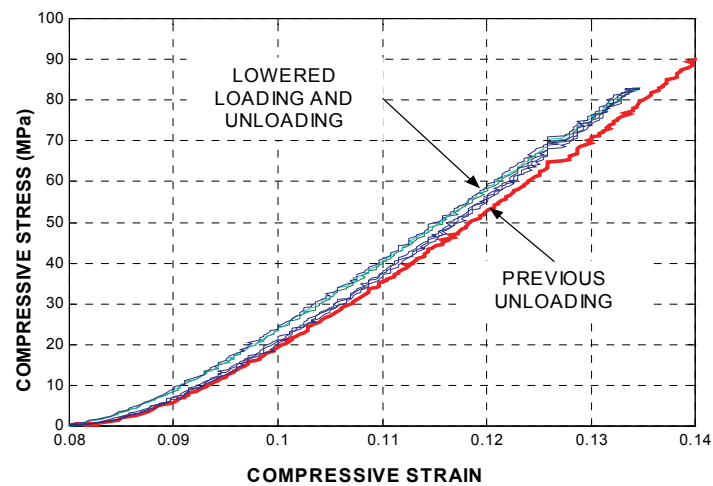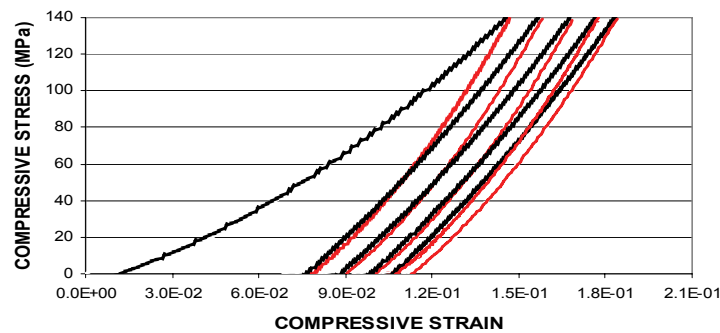

Figure 11. Detailed loading-unloading curves of the test using the first loading pattern (Mixing ratio: 0.77)
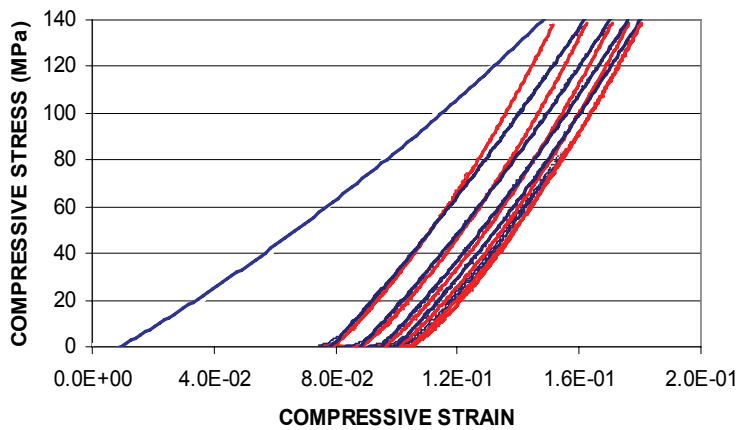
(a) Mixing ratio: 0.74
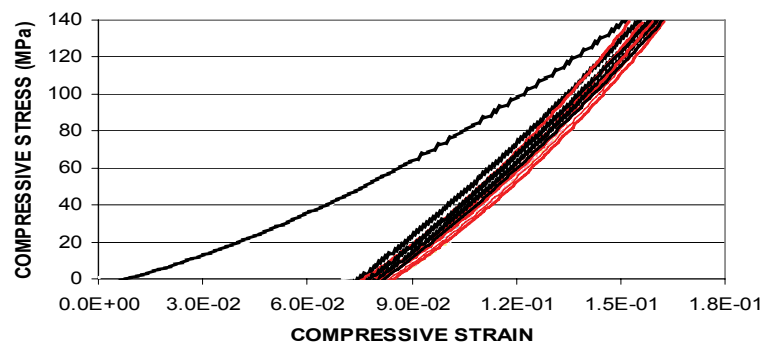
(b) Mixing ratio: 0.77

(c) Mixing ratio: 0.80

Figure 12. Loading-unloading curves using the second loading pattern

The increase in the total strain is less than 5% for the powder mixture with a mixing ratio of 0.77, indicating that the plastic deformation after the second loading cycle is very small.

4.5 Elastic Properties of Compacted Powders

Elastic properties, such as the Young's modulus and Poisson's ratio of compacted powders are important parameters for the deformation analysis of the metal shell and powder assembly used in the new RT process. Linear elasticity (Young's modulus and Poisson's ratio) is often sufficient to describe the behavior of compacted powders (Cambou, 1998). However, few studies have reported the elastic properties of unsintered compacted powders (Carnavas, 1998). Hehenberger *et al.* (1982) interpreted the unloading curves of uniaxial compression of compacted powders in terms of the Young's modulus and Poisson's ratio.

Powder/ Mixing ratio	Total strain			Compact density increase (%) between the second loading and the last loading
	Second loading (ε_S)	Last loading (ε_L)	$\Delta\varepsilon = (\varepsilon_L - \varepsilon_S)$	
T-15/0.80	0.157	0.183	0.026	8.1
T-15/0.77	0.155	0.162	0.007	0.6
T-15/0.74	0.162	0.179	0.017	1.8

Table 10. Changes of the total strain and compact density between the second loading and last loading

The Young's modulus and Poisson's ratios for the compacted binary T-15 powder mixture are obtained experimentally in this study using the data from the uniaxial compression test. The compaction of powders involves a number of different mechanisms. These mechanisms are interrelated through particle interactions that in turn depend on the distributed and individual particle properties. In contrast, unloading of the compacted powder is largely a linear elastic process. Therefore, the elastic properties of compacted powders can be more accurately determined from the elastic unloading process.

Typical unloading and reloading curves used for the calculation of the elastic properties of the compacted powder are shown in Fig. 13. Although the curves are not entirely linear, both the unloading and reloading curves have an apparently linear portion that is consistent with elastic deformation. In this linear portion, the reloading compressive strain does not exceed the previous unloading strain and the curve lies on the left of the previous unloading curve in the stress-strain diagram. In the current study, the elastic properties of compacted powders are calculated from the linear portion of the unloading curve. The linear portion is taken from the point with 20% of the maximum loading stress to the critical point. The elastic parameters of compacted powders are calculated using linear elastic theory. Figure 14 shows the unloading curve obtained from the compression test in the fifth unloading phase for the T-15 powder mixture with a mixing ratio of 0.77.

The Young's modulus of a compacted powder is calculated as follows:

$$E = \frac{\Delta\sigma}{\Delta\varepsilon} = \frac{\sigma_B - \sigma_A}{\varepsilon_B - \varepsilon_A} \qquad (4)$$

where σ is compressive stress [MPa] and ε is compressive strain. 'A' and 'B' could be any two points on the straight line as shown in Fig. 14. A linear regression analysis shows that the R-squared value for the curve shown in Fig. 14 is 0.9982. It indicates that the trend line of the selected segment matches well with the actual experimental data. The tangent of the trend line is 1679.8 MPa, which is the Young's modulus of the compacted T-15 powder mixture at a mixing ratio of 0.77.
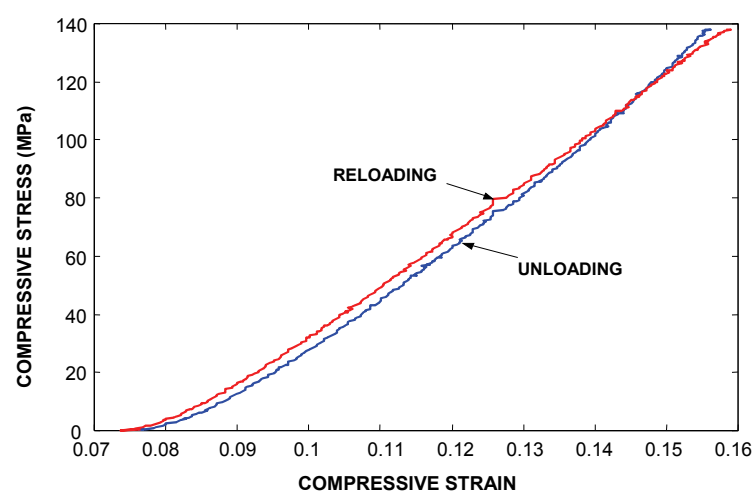

Figure 13. Typical unloading and reloading process
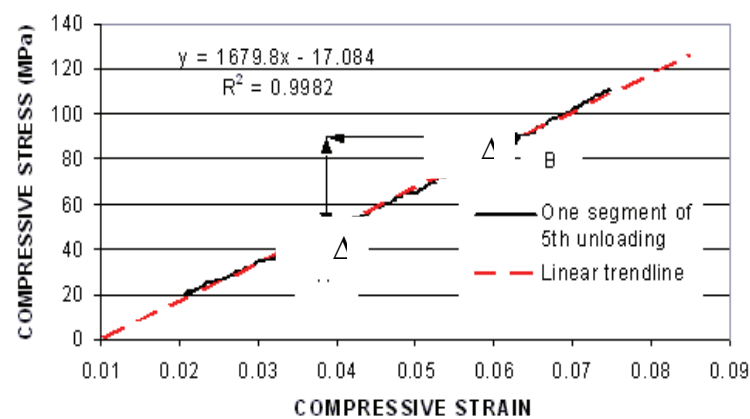
Figure 14. Selected unloading curve (Mixing ratio: 0.77)

For the calculation of the Poisson's ratio, it is assumed that the compression die is rigid, and the deformation on the inner surface of the die in the radial and circumferential directions is zero. From Hooke's Law, the triaxial stress can be written in cylindrical coordinates as (Gere, 2001):

$$\sigma_z = \frac{E}{(1+\nu)(1-2\nu)}\left[(1-\nu)\varepsilon_z + \nu(\varepsilon_r + \varepsilon_\theta)\right] \qquad (5)$$

where E is Young's modulus and ν is Poisson's ratio. When ε_r and ε_θ are equal to zero, Eq. (5) can be rewritten as:

$$\sigma_z = \frac{E}{(1+\nu)(1-2\nu)}(1-\nu)\varepsilon_z \qquad (6)$$

If the Young's modulus E is assumed to be a constant in Eq. (6), the compressive stress and strain have a linear relationship. Letting $\Omega = \dfrac{E\varepsilon_z}{\sigma_z}$, Eq. (6) can be rewritten as:

$$2\nu^2 - (\Omega-1)\nu + (\Omega-1) = 0 \qquad (7)$$

The values of the Poisson's ratio for the T-15 powder mixture at a mixing ratio of 0.77 are calculated based on the experimental data using Eq. (7). They are tabulated in Table 11 and shown in Fig. 15. The results show that the Poisson's ratio decreases with an increase in compressive stress. This agrees with the results from Hehenberger's study (1982). Since the Poisson's ratio is the ratio of lateral strain to axial strain during elastic deformation, the decrease in the Poisson's ratio with increasing stress means that the increments of lateral strain will become smaller with each increment of compressive stress (strain).

Compressive Stress σ_z (MPa)	Ω	Poisson's Ratio ν
110	0.8454	0.242
95	0.8210	0.258
80	0.7875	0.277
70	0.7570	0.293
55	0.6909	0.323
40	0.5750	0.367
25	0.3200	0.437

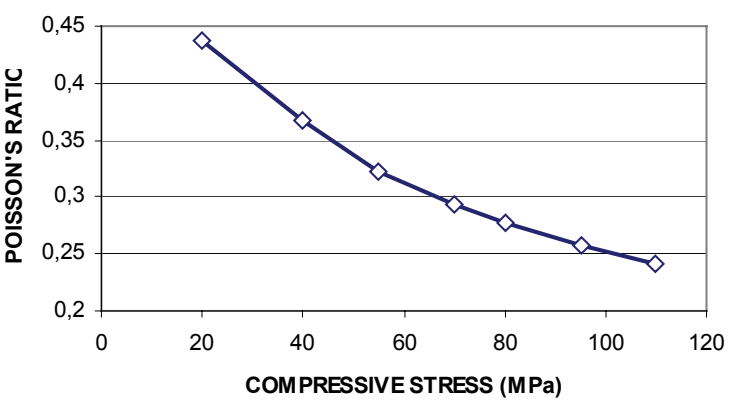Table 11. Poisson's ratios for T-15 tool steel powder mixture at the mixing ratio of 0.77

Figure 15. Variation of Poisson's ratio with compressive stress

5. Deformation of the Metal Shell

The front side of the metal shell used in the proposed new RT process has the shape complementary to the mould to be fabricated and the backside of the metal shell is hollow with a number of reinforcing ribs as shown in Fig 1. These ribs divide the space inside the metal shell into a number of square cells. The deformation analysis is conducted for a single cell formed by four adjacent ribs in the metal shell.
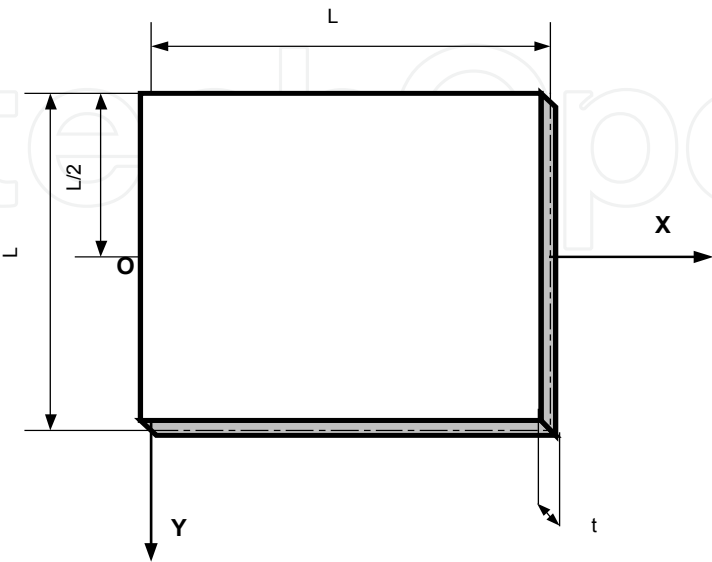

Figure 16. Dimensions of the thin plate

The ribs are assumed rigid and their deformation can be neglected during loading. Thus, the top surface of each cell can be considered as a thin plate with its four edges being clamped (fixed). Therefore, the model used for the deformation analysis of the metal shell is a square metal plate, which is equal to the size of a single cell, fixed at its four edges with a distributed force applied on it. This model is called the thin plate model. The dimensions of the thin plate are shown in Fig. 16, where *t* is the thickness of the plate and *L* is the edge dimension of the plate. The deformations of the thin plate can be analyzed using both the traditional elastic theory for a thin plate (Gould, 1998) and the finite element analysis (FEA) (Gould, 1998). Both methods are used in this study for the analysis of the deformation of the metal shell. The software I-DEAS (Lawry, 2000) is used for the FEA simulations. The comparison of the results from the two methods is presented.

5.1 Analysis Based on Traditional Elastic Theory

The assumptions used in traditional elastic theory for a thin plate are (Gould, 1998):

    a. The material of the plate is elastic, homogeneous, and isotropic.
    b. The plate is initially flat.
    c. The thickness "*t*" of the plate is small in comparison to its lateral dimension *L*. The smallest lateral dimension of the plate is at least ten times larger than its thickness, i.e. $t / L \leq 0.1$.
    d. Deformations are small in comparison to the thickness.

The maximum deformation occurs at the center of the plate. For a square plate with clamped edges, the maximum deformation based on the traditional elastic theory is (Gould, 1998):

$$\omega_{max} = 1.26 \times 10^{-3} \frac{p_0 L^4}{D} \qquad (8)$$

where

$$D = \frac{E t^3}{12(1 - v^2)}$$

ω_{max} is the maximum deformation of the plate, p_0 is the uniformly distributed load per unit area on the plate, E is the plate material elastic modulus, v is the plate material Poisson's ratio, and t is the thickness of the plate.

5.2 Analysis Based on FEA

The simulation function is used to conduct the finite element analysis. The three-dimensional solid element and free mesh method are used in the simulation so that there is no restriction on the thickness of the plate.

5.3 Results

Since the stress and deformation of the thin plate varies with the plate thickness and loading, the deformation analysis is carried out for a thin plate with different thickness as well as different loading using both the FEA and the traditional elastic theory. The dimensions of the plate are 25.4×25.4 mm^2 and the materials of the plate is nickel (E=210 GPa and v=0.31). Table 12 and Fig. 17 present the results on the maximum deformation of the metal shell at different relative shell thickness, t/L, with a uniformly distributed load of p_0 =138 MPa on the plate surface.

t (mm)	t/L	ω_{Max} (mm)		Difference (%)
		Elastic Theory	FEM Method	
0.2	0.0079	466.92	234	99.5
0.4	0.0157	58.37	48.9	16.2
0.6	0.0236	17.29	16.0	7.5
0.8	0.0315	7.30	6.98	4.4
1.0	0.0394	3.74	3.66	2.1
1.2	0.0472	2.16	2.15	0.5
1.4	0.0551	1.36	1.42	-0.04
1.6	0.0629	0.91	0.938	-3.1
1.8	0.0709	0.64	0.671	-4.8
2.0	0.0787	0.46	0.498	-8.3
2.4	0.0945	0.27	0.30	-11
2.8	0.1102	Not applicable	0.197	Not applicable
3.0	0.1181	"	0.165	"
3.4	0.1339	"	0.119	"
3.8	0.1496	"	0.091	"
4.0	0.1575	"	0.081	"
4.5	0.1772	"	0.062	"
5.0	0.1969	"	0.049	"

Table 12. Maximum metal shell deformation at different shell thickness

It can be seen that the thickness of the metal shell has a strong influence on the shell deformation. As shown in Fig. 17, when the relative shell thickness, *t/L*, is greater than 0.08, the deformation is not sensitive to the shell thickness. Table 12 shows that the maximum deformation calculated by both methods agree well in the range of *t/L* = 0.03 - 0.07, for which the difference between the two methods is less than 5%.

The smallest difference in the maximum deformation predicted by the two methods occurs at the relative thickness *t/L* = 0.055. In addition, when the relative thickness is greater than 0.1, the traditional elastic theory is not applicable for the prediction of the deformation. However, there is no such limitation for the FEA method using a three-dimensional element.

Table 13 shows the variation of the maximum deformation of the metal shell with loading at the relative shell thickness *t/L* = 0.0394. The results from both methods agree very well and the maximum difference is less than 2.3%.

6. Analysis of the Deformation of the Shell-Powder Assembly

The mechanical structure of the metal shell backfilled with the metal powder can be treated as a thin metal plate on an elastic block of compacted powders.

Loading (MPa)	ω_{max} (mm)		Difference (%)
	Elastic Theory	FEM Method	
137.9	3.74	3.66	2
124.1	3.36	3.29	2.1
110.3	2.98	2.93	1.8
96.5	2.61	2.56	2.1
82.7	2.24	2.19	2.3
68.9	1.87	1.83	2.0
55.2	1.49	1.46	2.3
41.4	1.12	1.10	1.8
27.6	0.747	0.731	2.2
13.9	0.374	0.366	2.0
6.9	0.187	0.183	2.0
3.4	0.0934	0.0914	2.1

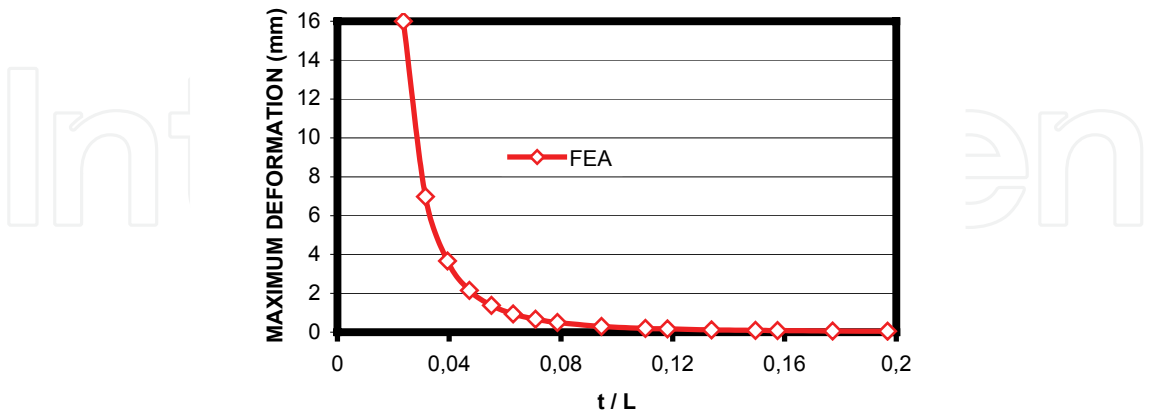Table 13. Maximum metal shell deformation at different loading

Figure 17. Variation of the maximum deformation of the shell with the shell thickness

Using the traditional elastic theory to analyze this type of structure is difficult although this is a common type structure in engineering applications. Therefore, the FEA method is used for the deformation analysis of the metal shell and powder assembly. The deformation behavior of the metal shell and powder assembly at different metal shell thickness, cell dimensions and compressive loading is investigated. The results can be used to optimize the structure of the shell-powder assembly.

6.1 Model and Boundary Conditions for the Shell-Powder Assembly

The analysis is carried out for a single cell of the metal shell and metal powder assembly. The model and the boundary conditions used in the analysis are shown in Fig. 18, where t is the thickness of the metal shell, H is the high of the powder, and L is the edge dimension of the cell. The material of the metal shell is nickel. The binary mixture of T-15 powders, Powders #5 and #7, at the mixing ratio of 0.77 is used to backfill the metal shell. The elastic properties of the binary powder mixture are from those given in Table 11. The boundary conditions of the model are also shown in Fig. 18. A uniform distributed stress, the loading, is applied on the top surface of metal shell. The four edge surfaces and the bottom of the shell-powder assembly are fixed.

6.2 Results

The simulations are performed for two different cell sizes of the shell-powder assembly, L=25.4 mm and L=12.7 mm, at different shell thickness, t, and differ-

ent loading, *P*. *H* is taken as 50 mm. The variations of the maximum deformation of the shell-powder assembly with the shell thickness and loading are shown in Fig. 19 for the cell size of *L*=25.4 mm and *L*=12.7 mm. It is observed that the cell size, *L*, and shell thickness, *t*, especially the cell size, significantly affect the deformation of the shell-powder assembly.
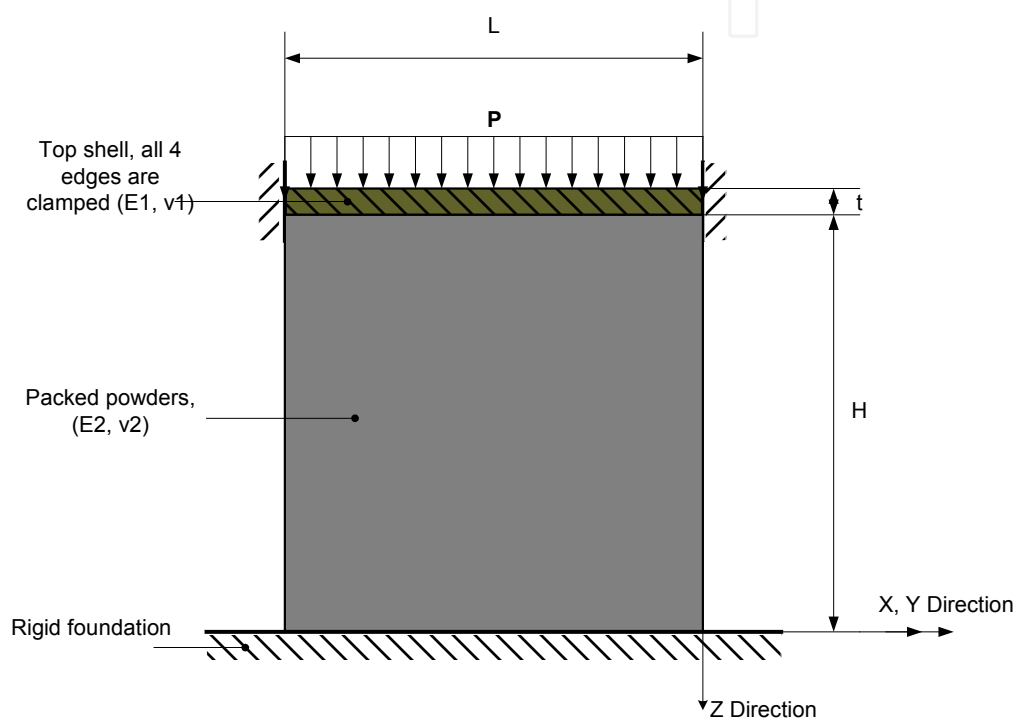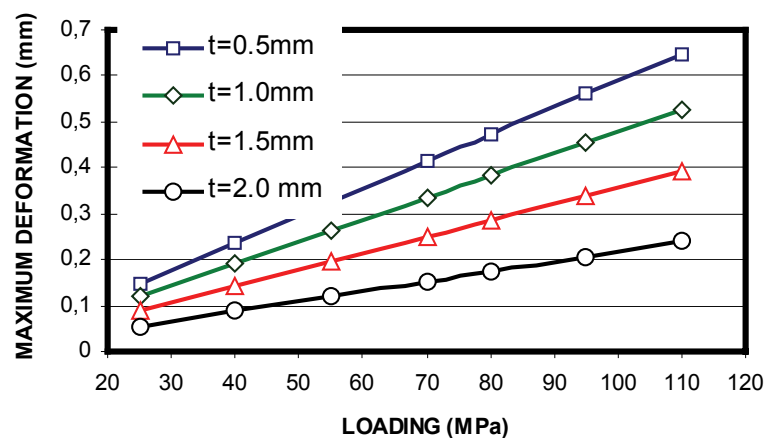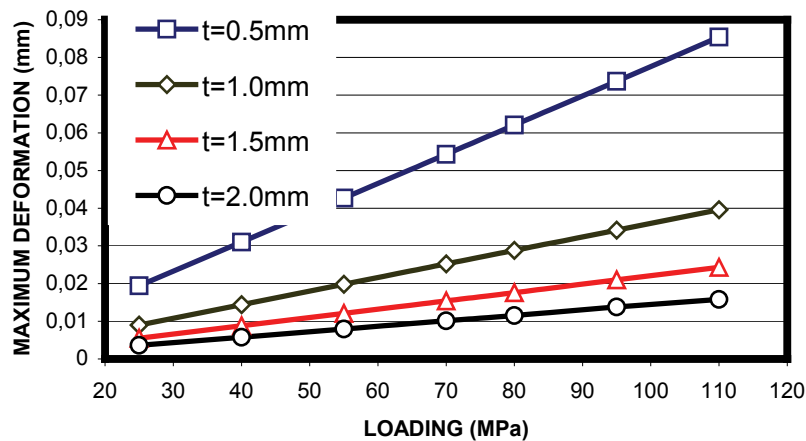

Figure 18. Shell-powder assembly and boundary conditions

(a) L = 25.4 mm

(b) L = 12.7 mm

Figure 19. Variation of the maximum deformation of the shell-powder assembly with the shell thickness and loading
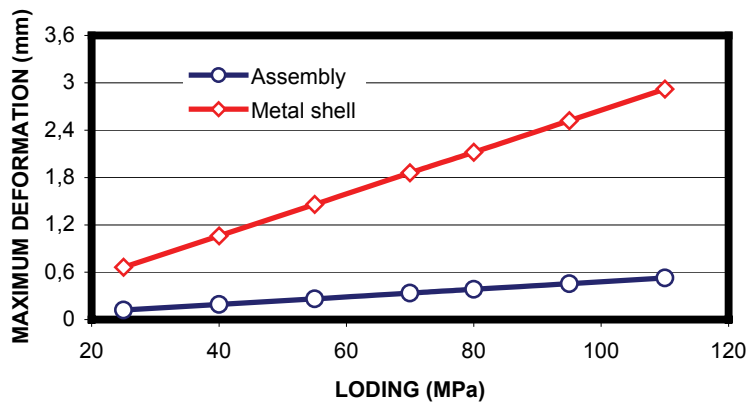
Figure 20. Comparison of the maximum deformations between the metal shell and the shell-powder assembly

At the same shell thickness, the maximum deformation can be lowered by a factor of 7-15 when the cell size is reduced from 25.4 mm to 12.7 mm.

For the same cell size, the maximum deformation can be lowered to 2.7 and 5.3 times when the shell thickness is increased from 0.5 mm to 2 mm.

The comparison of the maximum deformation of the metal shell and the shell-powder assembly is given in Fig. 20, where the parameters are H=50 mm, L=25.4 mm, and t=1 mm. It can be seen that the use of the backfilled metal powder greatly improves the structure's ability to resist deformation. The

maximum deformation of the shell-powder assembly at a compressive loading of 110 MPa is only 18% that of the metal shell without the powder backing support. Without powder support, the maximum deformation of the metal shell increases drastically with the increase in loading as shown in Fig. 20. In contrast, the increase in the maximum deformation with the increase of the loading is very slow if the back support metal powder is used.

7. Conclusions

In the single component packing, the particle shape has the most significant effect on the powder packing density. The spherical and round particles produce higher packing density, and therefore, are desirable for the intended RT application. The dimension ratio of the container and the particle (D/d) has less effect on the packing density when $D/d \geq 7.66$, but packing density started to drop significantly when the ratio D/d is less than 5. The particle size has no significant effect on the packing density. Mixing particles with different sizes can greatly increase the packing density because the voids among large particles can be filled by small particles. In the current study, the packing density of three-component packing can reach 0.91 and binary packing density can reach 0.86. The particle size ratio is a very important parameter for multiple component packing. For best packing results, the size ratio of the large particle to the small particle should be higher than at least 6.82 so that all small particles can enter the interstices between large particles. On the other hand, particle size should not be too small to avoid low fluidity. The mixing ratio is another important parameter affecting multiple component packing density. There exists an optimal mixing ratio for a binary mixture at which the packing density is maximal. The optimal mixing ratio is in the range of 0.71 - 0.77.

The deformation behavior of compacted powders under uniaxial compression depends heavily on the properties of the powder materials, the mixing ratio of powders of different sizes, as well as the loading history. It is possible to obtain the required elastic properties of the compacted powders used for the proposed RT application by adjusting these factors. The powder with the higher hardness has less compressive deformation under the same loading conditions. Higher hardness also helps to prevent compacted powders from forming blocks after compression, which is necessary for powder reuse. The T-15 tool steel powder is the best choice among the materials studied for the proposed new RT process. In addition, the mixing ratio of 0.77 is found to

give the highest deformation resistance. The critical point is an interesting and important phenomenon for powder compression. It defines the limit for the operating load that produces the smallest increase in plastic strain under the tool working condition. The loading history is important for the deformation behavior of compacted powders. A higher loading stress level generally leads to higher operating loads without further plastic deformation in subsequent loading. The load level that corresponds to the critical point increases with the number of loading cycles. The deformation resistance of the compacted powder can be improved by increasing the number of loading cycles. The unloading curves have a linear portion and are almost parallel in a certain range of the stress-strain curve. The Young's modulus and Poisson's ratios can be obtained using the experimental data from the linear portion.

The maximum deformation of the metal shell predicted by the elastic theory and FEA method are in good agreement in a certain range of the relative shell thickness (t/L). The elastic theory is applicable only for a thin plate. However, there is no such restriction for the FEA method. The relative metal shell thickness has a significant effect on the deformation of the metal shell. Furthermore, the use of the metal powder to support the metal shell can greatly improve its ability to resist deformation. The deformation of the metal shell-powder assembly depends also strongly on the dimension of the cell size and the thickness of the metal shell. Use of a proper cell dimension and shell thickness can limit the deformation of the shell-powder assembly within the tolerance, which indicates that the proposed new rapid tooling process is feasible.

8. References

ASTM B331-95 (2002). *Standard Test Method for Compressibility of Metal Powder in Uniaxial Compaction*, ASTM International.

Cambou, B. (1998). *Behavior of Granular Materials*, Springer Verlag.

Carnavas, P. C. (1998). Elastic Properties of Compacted Metal Powders, *Journal of Material Science*, Vol. 33, pp. 4647-4655.

Gere, J. M. (2001). *Mechanics of Materials*, 5th edition, Brooks/Cole, Pacific Grove, CA.

German, R. M. (1998). *Powder Metallurgy of Iron and Steel*, John Wiley & Sons Inc., New York.

Gould, P. L. (1998). *Analysis of Shells and Plates*, Prentice Hall Upper Saddle River, New Jersey.

Hehenberger, M., Samuelson, P., Alm, O., Nilsson, L. and Olofsson (1982). Experimental and Theoretical Studies of Powder Compaction, *Proceedings of the Conference on the Deformation and Failure of Granular Materials*, IUTAM, pp. 381–390, Delft, September, 1982.

Hejmadi, U., and McAlea, K. (1996). Selective Laser Sintering of Metal Molds: The Rapid Tooling Process, *Proceedings of the Solid Freeform Fabrication Symposium*, pp. 97-104, Austin, TX, August, 1996.

Jacobs, P. F. (1992). Rapid Prototyping & Manufacturing Fundamentals of Stereo Lithography, Society of Manufacturing Engineers, Dearborn, MI.

Lawry, M. H. (2000). I-DEAS Master Series™ (Mechanical CAE/CAD/CAM Software), *Student Guide*, Structural Dynamics Research Corporation, Eastman Dr. Milford, OH.

Leva, M. and Grummer, M. (1947). Pressure Drop Through Packed Tubes, Part III, Prediction of Voids in Packed Tubes, *Chemical Engineering Progress*, Vol. 43, pp. 713-718.

McGeary, R. K. (1962). Mechanical Packing of Spherical Particles, *Journal of the American Ceramic Society-McGary*, Vol. 44, No. 10 pp. 513-522.

Nelson, C. (1999). Rapid Tooling Mold Inserts for Pressure and Gravity Die Casting Using SLS Technology, *Transactions of World of Die Casting*, Nov., pp. 441-446.

Pham, D. T. (1998). Techniques for Firm Tooling Using Rapid Prototyping, *Proceeding of the Institution of Mechanical Engineers, Part B: Journal of Engineering Manufacture*, Vol. 212, No. B4, pp. 269-277.

Phelan, M. (1997). The Two-Week Tool, *Automotive Industries*, March, pp. 62-63.

Shinohara, K. (1984). Rheological Property of Particulate Solids, *Handbook of Powder Science and Technology*, New York, pp. 396-404.

Willis, S. (1997). Fast Rapid Tooling for Injection Molds, *Proceedings of the Seventh International Conference on Rapid Prototyping*, pp.1-12, San Francisco, March, 1997.

Manufacturing the Future

Edited by Vedran Kordic, Aleksandar Lazinica and Munir Merdan

The primary goal of this book is to cover the state-of-the-art development and future directions in modern manufacturing systems. This interdisciplinary and comprehensive volume, consisting of 30 chapters, covers a survey of trends in distributed manufacturing, modern manufacturing equipment, product design process, rapid prototyping, quality assurance, from technological and organisational point of view and aspects of supply chain management.

How to reference

In order to correctly reference this scholarly work, feel free to copy and paste the following:

INTECH
open science | open minds